The UA9 experimental layout

2011 JINST 6 T10002

(http://iopscience.iop.org/1748-0221/6/10/T10002)

Jinst

PUBLISHED BY IOP PUBLISHING FOR SISSA

RECEIVED: *September 13, 2011*
ACCEPTED: *September 27, 2011*
PUBLISHED: *October 13, 2011*

TECHNICAL REPORT

The UA9 experimental layout

W. Scandale,[a,b,f] G. Arduini,[a] R. Assmann,[a] C. Bracco,[a] F. Cerutti,[a] J. Christiansen,[a] S. Gilardoni,[a] E. Laface,[a] R. Losito,[a] A. Masi,[a] E. Metral,[a] D. Mirarchi,[a] S. Montesano,[a] V. Previtali,[a] S. Redaelli,[a] G. Valentino,[a] P. Schoofs,[a] G. Smirnov,[a] L. Tlustos,[a] E. Bagli,[c] S. Baricordi,[c] P. Dalpiaz,[c] V. Guidi,[c] A. Mazzolari,[c] D. Vincenzi,[c] S. Dabagov,[d] F. Murtas,[d] A. Carnera,[e] G. Della Mea,[e] D. De Salvador,[e] A. Lombardi,[e] O. Lytovchenko,[e] M. Tonezzer,[e] G. Cavoto,[f,1] L. Ludovici,[f] R. Santacesaria,[f] P. Valente,[f] F. Galluccio,[g] A.G. Afonin,[h] M.K. Bulgakov,[h] Yu.A. Chesnokov,[h] V.A. Maisheev,[h] I.A. Yazynin,[h] A.D. Kovalenko,[i] A.M. Taratin,[i] Yu.A. Gavrikov,[j] Yu.M. Ivanov,[j] L.P. Lapina,[j] V.V. Skorobogatov,[j] W. Ferguson,[k] J. Fulcher,[k] G. Hall,[k] M. Pesaresi,[k] M. Raymond,[k] A. Rose,[k] M. Ryan,[k] O. Zorba,[k] G. Robert-Demolaize,[l] T. Markiewicz,[m] M. Oriunno,[m] U. Wienands,[m]

[a] *CERN, European Organization for Nuclear Research, CH-1211 Geneva 23, Switzerland*

[b] *Laboratoire de l'Accélérateur Linéaire (LAL), Université Paris-Sud 11, Centre Scientifique d'Orsay, B.P. 34, F-91898 ORSAY Cedex, France*

[c] *Universitàa di Ferrara, Dipartimento di Fisica and INFN, via Saragat, 1 I-44122 Ferrara, Italy*

[d] *INFN — Laboratiori Nazionali di Frascati, Via E. Fermi, 40 00044 Frascati Roma Italy*

[e] *INFN — Laboratori Nazionali di Legnaro, Viale Università 2, 35020 Legnaro PD, Italy*

[f] *INFN — Sezione di Roma, Piazzale Aldo Moro 2, 00185 Rome, Italy*

[g] *INFN — Sezione di Napoli, via Cintia, I-80126, Napoli, Italy*

[h] *Institute of High Energy Physics, Moscow Region, RU-142284 Protvino, Russia*

[i] *Joint Institute for Nuclear Research, Joliot-Curie 6, 141980, Dubna, Moscow Region, Russia*

[j] *Petersburg Nuclear Physics Institute, PNPI Gatchina, St-Petersburg 188300, Russia*

[1] Corresponding author.

doi:10.1088/1748-0221/6/10/T10002

[k]*Imperial College, Imperial College London,*
SW7 2AZ London, U.K.
[l]*Brookhaven National Laboratories,*
P.O. Box 5000 Upton, NY 11973-5000, U.S.A.
[m]*SLAC National Accelerator Laboratory,*
2575 Sand Hill Road Menlo Park, CA 94025, U.S.A.

E-mail: gianluca.cavoto@roma1.infn.it

ABSTRACT: The UA9 experimental equipment was installed in the CERN-SPS in March '09 with the aim of investigating crystal assisted collimation in coasting mode. Its basic layout comprises silicon bent crystals acting as primary collimators mounted inside two vacuum vessels. A movable 60 cm long block of tungsten located downstream at about 90 degrees phase advance intercepts the deflected beam. Scintillators, Gas Electron Multiplier chambers and other beam loss monitors measure nuclear loss rates induced by the interaction of the beam halo in the crystal. Two Roman pots installed in the path of the deflected particles are equipped with a Medipix detector to reconstruct the transverse distribution of the impinging beam. Finally UA9 takes advantage of an LHC-collimator prototype installed close to the first Roman pot to help in setting the beam conditions and to analyze the efficiency to deflect the beam. This paper describes in details the hardware installed to study the crystal collimation during 2010.

KEYWORDS: Accelerator Subsystems and Technologies; Beam-line instrumentation (beam position and profile monitors; beam-intensity monitors; bunch length monitors); Instrumentation for particle accelerators and storage rings - high energy (linear accelerators, synchrotrons)

2011 JINST 6 T10002

Contents

2011 JINST 6 T10002

1 Introduction

Halo particles in circular accelerator represent a threat for the good performance, stability and protection of the machine. A specific beam collimation system must be designed and implemented based on passive objects able to scatter and absorb undesired particles at the peripheral of the circulating beam. In the last years bent crystals have been efficiently used to extract beam particles out of an accelerator [1] using the coherent interaction of the charged particles with the crystal (*crystal channeling*). Crystal extraction can be applied to the main beam but also to halo particles [2]. A crystal assisted collimation system for hadron colliders (as the Large Hadron Collider, LHC) has been proposed [3].

A classic two-stage collimation system [4] in accelerators consists of a primary element acting as a small scattering target and a secondary element absorbing particles impinging on it. The LHC collimation systems is based on these concepts [5] . An amorphous primary target scatters particles in no preferred direction while a bent crystals traps particles with the coherent scattering on aligned atomic planes and kicks them in only one direction. The halo protons can be redirected so that they hit the secondary absorber with a large impact parameter and therefore can be efficiently removed.

CERN approved in 2008 the UA9 experiment with the aim of testing directly the crystal assisted collimation as an alternative for both protons and lead ion beam collimation in the LHC.

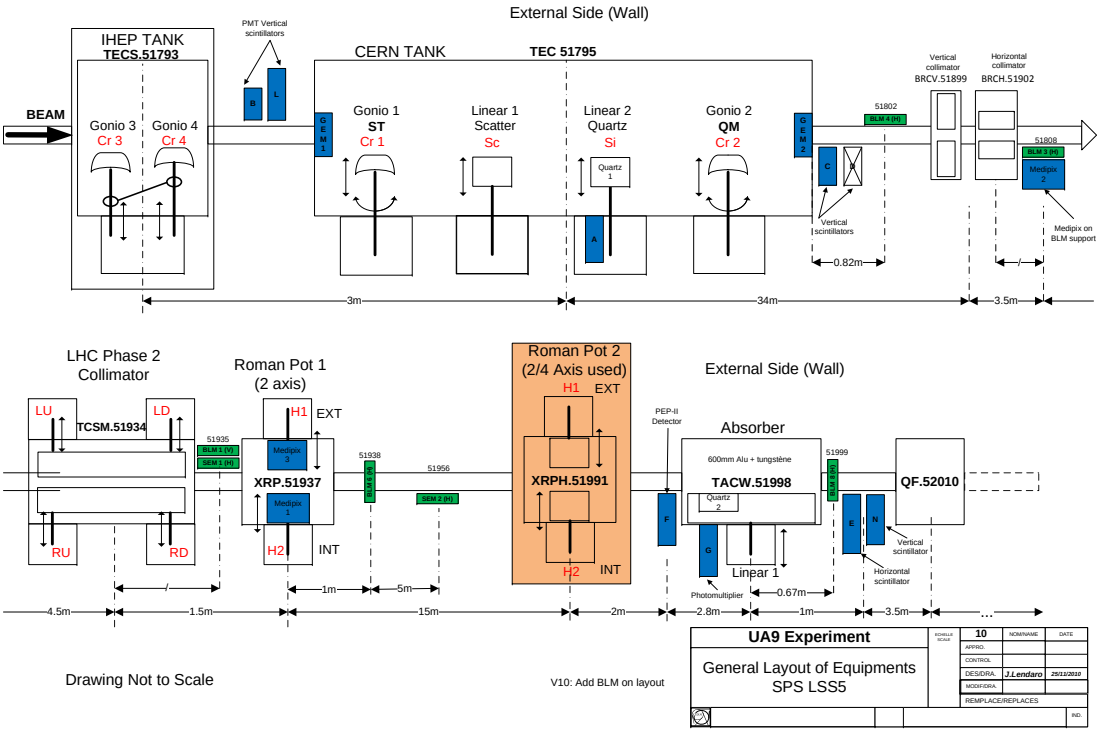

Figure 1. UA9 collimation region layout as in 2010 data-taking.

UA9's final goal is to demonstrate that crystal based collimation has a higher cleaning efficiency than traditional scheme. This paper focuses on the layout of the UA9 equipment installed in the SPS ring. Various beam instrumentation and detectors are in fact used to measure the beam losses close to the crystal and around the ring with different level of accuracy and redundancy. The procedures to detect and establish the channelling condition and to measure the collimation efficiency are subjects of other publications.

2 The experimental region

In this paper we describe the UA9 layout, located in the Long Straight Section 5 of the SPS, that was set in place for the 2010 data-taking. The full layout is schematically shown in figure 1 and figure 2 respectively. Each box describes either a UA9 device or an accelerator component, also indicating the official SPS acronyms, such as TECS.51793, TEC.51795, BRCV.51899 and so on. These acronyms, made of 3 or 4 letters and 5 numbers, are intended to specify the functionality and the location of each device, according to a conventional dictionary.

In figure 1 the instrumented beam line is shown where the beam cleaning devices are sitting, the losses should be concentrated and the beam detectors are densely packed (the *collimation region*). Four silicon crystals ("Cr1" to "Cr4") mounted on precision goniometers ("Gonio1" to "Gonio4") are installed in two vacuum vessels named "IHEP tank" and "CERN tank" respectively. The first tank was manufactured for UA9 at Institute for High Energy Physics in Protvino, Russia

2011 JINST 6 T10002

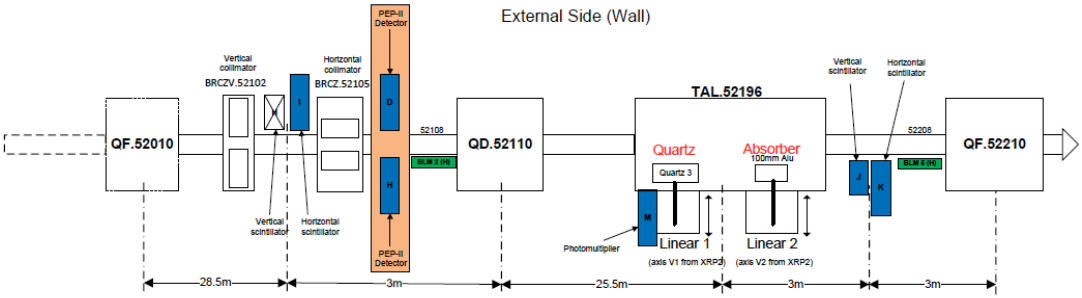

Figure 2. External beam dump in UA9 layout.

and the second originally belonging to the RD22 experiment was recently refurbished at CERN. Each crystal can be independently used as primary halo deflector. Inside the CERN tank a tungsten scatterer and a Cherenkov detector are mounted, the first to make direct measurement with an amorphous material used as primary collimator and the second to quantify the number of impinging particles on the crystal 2 (Cr2). Channeled protons are coherently deflected by the angle given by the crystal bending angle (around 160 μrad). About 60 m downstream of the crystals (position "TACW.51998") the channeled protons are displaced by several mm with respect to the primary beam envelope and they are then collected on a 60 cm long secondary tungsten collimator, instrumented with another Cherenkov detector. In close proximity and outside of the vacuum vessels some detectors are installed which are sensitive to the production of secondary particles from inelastic interactions in the obstacles present within the beam pipe. Several scintillators counters equipped with PMTs, Gas Electron Multiplication chambers (GEM) and LHC-type ionization chamber Beam Loss Monitor (LHC BLM) are used for this purpose. About 45 m downstream of the crystals a Roman Pot device (RP1, at "XRP.51937") is installed. It comprises two horizontal axes with linear motors (H1 and H2 in figure 1). Each axis supports a secondary vacuum vessel containing one Medipix [6] pixel detector that can be moved towards the center of the beam to intercept the channeled beam and to provide an online image of it during data-taking. The secondary vacuum vessels that separate the detectors from the primary beam vacuum have 0.2 mm thin aluminium walls and are 3.4 cm wide in the beam direction. They could generate secondaries when moved into the beam, especially from the bottom wall that is parallel to the incident particle direction. In operation however, the bottom wall should sit in the gap between the circulating and the deflected beam where the particle density is low and the secondary spray strongly reduced. A second Roman Pot (at "XRPH.51991") has been more recently installed; it features four axes (two horizontal and two vertical) and it will be used in the next data taking sessions when detectors are installed inside its four vessels. Few meters upstream of the RP1 a LHC-phase-2 collimator is installed and used to cut portion of the beam and derive measurements of the channeled beam.

Figure 2 shows the UA9 devices located about 120 m downstream of the crystals where the dispersion function is approaching its maximal value and the detection of the off-momentum halo is optimal. Off-momentum halo particle population is likely to be enhanced by the collimation process itself. Single diffractive events in the primary collimator may indeed leave unchanged the trajectory and substantially reduce the energy of the incident particles, thereby preventing the

2011 JINST 6 T10002

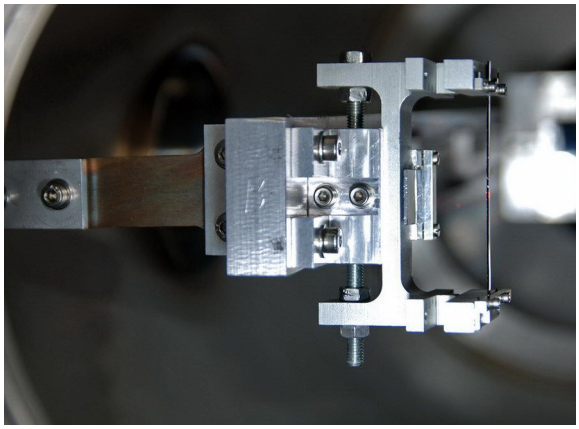

Figure 3. Cr1 strip crystal in CERN tank.

secondary absorber to collect them. Those particles are unavoidably lost as soon as the dispersion function increases. In bent crystals, nuclear interactions are substantially reduced [7]. So should be the diffractive interactions and the population of self-generated off-momentum halo. One of the main goals of UA9 is to directly check whether this is true when using bent crystals as primary collimators. In the location "TAL.52196" of figure 2, a 10 cm long duralumin bar can be used as a scraper to intercept off-momentum particles that are likely to be generated in the interaction with the crystals. Here the efficiency of the collimation system can be evaluated by detecting the scattered protons. Scintillators and Cherenkov detectors are installed nearby to intercept the secondary particles produced by the protons inside the Al bar.

SPS was available to UA9 experiment during five dedicated machine development periods lasting 24 hours each during the 2010. The machine was operated in coasting mode with 120 or 270 GeV beams, depending on the run, made of one single bunch that at the start of the fill contained about 10^{11} protons. One crystal at a time was set at the edge of the circulating beam and became the primary collimator. Measurements could be performed that included the angular scan of the selected crystal and scans with various absorbers. In stationary condition protons from the beam halo are diffusing into the edge of the crystal with a rate such that around 100 protons are reaching the crystal at every turn (23 μs) within the bunch time length (3 ns). This time structure of the halo protons is reproduced in the signals seen by the various detectors.

2.1 Crystals

Crystals fully appropriate for halo collimation in high energy hadron colliders are the result of a long optimization process. Silicon is the preferred material to produce large dislocation-free crystal plates, precisely cut with the faces parallel to (110) or (111) planes, within a hundreds of μrad and with the beam face properly etched and optically polished. Short crystals of a few mm or a few fractions of mm length allow extending the range of energy, in which crystals have large channelling efficiency [8]. A constant curvature obtained through the elastic property of the crystal itself avoids local perturbations of the bending radius that are eventually introduced whenever external supports are used to impart the flexural stress on the face exposed to beams, thereby reducing the channelling probability [9]. Finally a procedure for the removal of the amorphous layer at the

2011 JINST 6 T10002

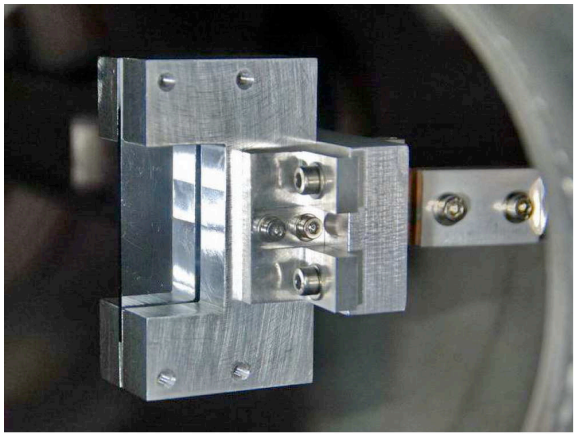

Figure 4. Cr3 quasimosaic crystal in IHEP tank.

crystal surface implies the possibility of channelling as soon as the particles hit the crystal surface, which is a mandatory request when particles intersect the crystal at a small grazing angle. Strip crystal plates of one to a few mm thickness have been cut along the (110) planes and bent as to produce an homogeneous anticlastic curvature [10] of the order of or larger than a few hundred μrad [11]. The primary curvature imparted to bend the strip crystal by the mechanical holder induces a secondary curvature due to anticlastic deformation.[1] This secondary deformation is used to steer incoming particles along the crystal planes. Anticlastic deformation also enables to set the metallic components of the holder far from centre of the crystal and in turn far from the beam ([12] and see figure 1 therein). Should the two edges of a strip crystal be constraint along non-parallel directions, then the flexural stress imparted by the holder would induce in the different portions of the strip an anticlastic reaction with a saddle shape slowly rotating as a function of the distance from the strip edges. This should induce a torsion of the crystal shape along the strip axis and a different path to channeled particles hitting the strip at different heights. Appropriate pre-adjustment of the holder may mitigate such a detrimental effect. Shorter crystals of a few tenths of mm length have also been cut along the (111) with the external faces parallel to the atomic lattice and bent by hundreds of μrad through the quasi-mosaic elastic effect [13]. A holder imparts to the largest crystal face a mechanical curvature along one dimension that produce the anticlastic reaction along the other dimension and the saddle shape of the face. The quasi-mosaic reaction along the third dimension (in general the shortest) induces a cylindrical shape deformation to the crystal planes. The deformation results from the anisotropic elastic reaction of crystal planes to the mechanical flexural stress imposed to its main axis. Also in this case the cylindrical shape of the crystal planes cannot be perfectly parallel in the space. A slow rotation of the cylindrically bent crystal planes along the anticlastic curvature is unavoidable. Such an effect can only be mitigated by a proper choice of the crystal plate dimension and of the main bending angle. For all crystal types the miscut, which is the angle of the crystal face exposed to the beam with the crystal planes, should be minimal to allow the full deflection of the incoming particles even when they hit the crystal at

[1] When elastic strips are bent, the longitudinal strains, which are purposely induced, are accompanied by lateral strains in the width direction of the strip. As a result, the strip takes the shape of a saddle, i.e., it bends to a surface in which the two principal curvatures are opposite in sign. This effect is referred to as anticlastic deformation.

2011 JINST 6 T10002

Figure 5. IHEP (to the left) and CERN (to the right) tanks.

small grazing angles. Any residual miscut imply that particles approaching the bent crystal with a small impact parameter may be only partially deflected and therefore lost in sensitive area of the accelerator instead than in the secondary absorber ([14] and figure 3 therein).

The crystal Cr1 has been largely used for channeling and volume reflection studies [15] by the UA9 collaboration and top performed in efficiency (83%) with a low-divergence beam. Bending angle of Cr1 crystal have been characterized by means of white light interferometry (Veeco NT1100) and resulted to be 160 μrad, while miscut angle have been measured by means of a Panalytical high resolution X-ray diffractometer and resulted to be about 150 μrad. The relative angular errors were of the order of a tens of percent. Over a thickness of 2 mm a miscut angle of 100 μrad generates a region of reduced channeling efficiency as wide as 0.2 μm. For Cr4, the holder has been equipped with a mechanical system to compensate for torsion in the strip crystal thanks to a feedback method during the standard stage of quality check of the crystal at fixed-target experimental area [16]. Crystal miscut resulted to be 200$\pm$20 μrad. Both crystal torsion and bending angle (176 μrad) have been measured through deflection under planar channeling regime of a 400 GeV protons beam, available at SPS-H8 line. Crystal torsion, arising as a consequence of holder mechanical imperfections, has been reduced to 0.6 μrad/mm.

The quasi-mosaic crystals Cr2 and Cr3 (shown in figure 4) have been fabricated by Petersburg Nuclear Physics Institute (PNPI). The crystals are deeply polished with submicron abrasive and slow etching: this yields a perfect plane crystalline surface covered by several fine grooves. They have a larger transverse section than strip crystals but similar thickness in the direction parallel to the beam ($18 \times 15 \times 1.6$ mm^3 and $30.5 \times 57.5 \times 2.10$ mm^3, respectively). Their bending angles are measured with optical systems to be 150 and 165 μrad and their miscut angles are 43 μrad and 92 μrad respectively. They are installed in rigid holder frames that leave only a fraction of their transverse section to be exposed to the beam (2×10 mm^2 and 20×40 mm^2 respectively). Torsional effects induced by the holders have been measured with optical system to be in the range 2–5 μrad/mm depending on the vertical position on the crystals.

2.2 Goniometers

In the primary vacuum of CERN tank at "TEC 51795" two high precision goniometers are installed. They allow a linear movement perpendicular to the beam in order to insert the crystals into the beam

2011 JINST 6 T10002

Figure 6. IHEP tank with autocollimator.

and they generate a rotation in the horizontal plane. Crystals Cr1 and Cr2 are installed on these two goniometers. In the IHEP tank at "TECS.51793" - that is located 3 m upstream the CERN tank - another mechanical system to which Cr3 and Cr4 are connected is placed in the primary vacuum. In this case the crystals are mounted on two mechanically connected supports that allow horizontal linear movement of each crystal: when one of the crystals is placed at a fixed distance from the beam, it can be rotated by applying a linear movement to the other support. In figure 5 the series of the two tanks is showed. Both systems can rotate the crystal in angular range of tens of mrad. They were designed to have a resolution (minimum step achievable by the motor) of 1 μrad and an accuracy (precision to which the motor goes to a given angular position) close to 10 μrad but such performances were only partially reached during data-taking. In all goniometers the linear position of a pushing system (measured with LVDT) is transformed to the crystal angle via a gear box with some error. All goniometers are different but can be characterized by the ratio of the real angular step measured with an optical laser autocollimator (figure 6) to the value of the step in the motion controller. Such calibration were done in laboratory and directly in situ through optical windows that are available in the CERN and IHEP tank. During angular scan in which the crystal is rotated with a fixed angular velocity (1–10 μrad/sec) the angular step calculated from LVDT readings was compared with the average angular step over one second. Average deviations from linearity were measured and accounted for with an ad-hoc model. From the RMS deviation from linearity we estimate an accuracy of 10 μrad over an angular range of 15 mrad.

2.3 Absorber

The absorber (at "TACW.51998") is a 60 cm long tungsten bar (figure 7) with a 7×6 cm^2 section located in a vacuum tank. It can be moved directly in and out of the beam and therefore acts as secondary collimator in all the measurements performed. Finite Element simulations have shown that the inefficiency in stopping protons in the range of energies used in the UA9 runs is of a few per mille. A quartz crystal covering partially the bar entrance face generates Cherenkov light that is transported in the same crystals to a PMT. The light emitted is proportional to the number of crossing protons and can be therefore used to measure the channeling efficiency in this collimation system. The Cherenkov detector signal is acquired and digitized with an amplitude to frequency converter within a gate generated synchronously to the RF SPS signal. This is therefore designed

2011 JINST 6 T10002

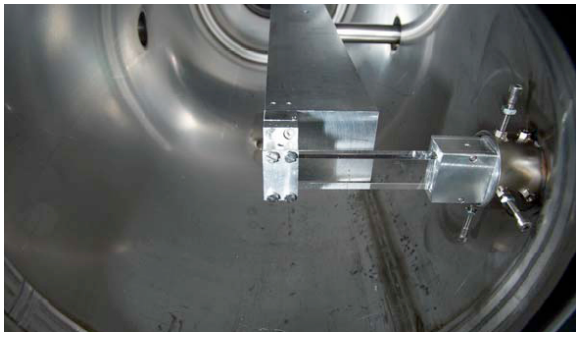

Figure 7. Tungsten absorber at TACW.51998 with quartz Cherenkov radiator. The radiator is clamped to the tungsten bar to the left and can slide though the left support whilst the absorber is moving. The sliding box ends with a window through with the Cherekov light can be collected.

to count protons originated from the single bunch time structure of the beam. Outside the vacuum tank scintillator detectors are installed which are sensitive to secondary particles produced in the hadronic showers and are therefore used to indirectly monitor the channeled beam.

2.4 LHC-type collimator

The LHC-type collimator ("TCSM.51934") is a full-scale prototype of the LHC Phase II secondary collimator and has two horizontal, one-meter long copper "jaws". The position and longitudinal tilt angle of each jaw can be controlled independently by means of four precise stepping motors (two per jaw) with minimum step size of 5 μm. The jaw positions are calibrated with respect to the nominal beam center and can be moved across the beam by 5 mm. The maximum collimator gap with fully retracted jaw is 60 mm. The two-sided collimator design allows to precisely define the beam envelope by closing the jaws around the circulating beam orbit and to identify its center. The collimator was also used to scan of the beam deflected by the crystal, in order to measure the channelling efficiency. The protons interacting in the jaws are producing secondaries that are seen by LHC-type beam loss monitors located downstream.

3 Beam loss monitors

Protons circulating in the accelerator hit obstacles and are therefore either deflected, or lose part of their energy or undergo inelastic interactions with nuclei. Detectors sensitive to showers of secondaries produced in such interactions are placed along the beam line to measure the rate of such interaction. We generically indicate them as beam loss monitor (BLM). Different type of detectors were used with different sensitivity to various range of interaction rates.

3.1 Scintillators

Polystirene scintillator slabs with different sizes are mounted outside the beampipe on mechanical supports at critical locations of the layout. They have an approximately 10×10 cm^2 square shape with a thickness of 0.5–1.5 cm. They are read out with conventional photomultipliers (PMT) connected to them via a light guide. Six of them are installed in pairs on the same support in a way coincidence of signals from the two PMTs can be used to suppress low energy background. Two

2011 JINST 6 T10002

more single scintillator counters are used to monitor indirectly the beam losses. Those scintillators are mostly sensitive to the charged component of the hadronic shower originating from proton interaction in either crystals or collimator jaws. During 2010 data-taking the PMT signals were discriminated with a relatively high threshold corresponding to several minimum ionizing particles (mips) energy release. The discriminated signals were fed into scaler's channels to count hits in a gate of 20 ms fixed length. The data acquisition system was realized with standard VME protocol in a Labview framework. In the proximity of crystals scintillators counting rates in the crystal amorphous orientation were in the range of 1–10 KHz depending of machine fill conditions. Given the time structure of the beam (one single bunch) several protons are hitting the crystals or other obstacles within few ns. Since no pulse height information is retained scintillators are not able to separate the contribution of the single protons and therefore their counting rate tend to saturate at the machine revolution frequency (43 KHz). They were especially useful during the online data analysis to find the crystals channeling condition and in offline analysis to determine the beam loss patterns in channeling versus amorphous condition.

3.2 PEP-II-type detectors

The PEP-II beam-loss monitors [17] are detecting Cherenkov light using a 16-mm photomultiplier with about 2 ns intrinsic pulse width. The radiator is an 8 mm diameter, 10 mm long fused-silica cylinder placed against the fused-silica PMT window with optical grease on the interface. The opposite end and the cylindrical surface are aluminized for high reflectivity. The assembly is enclosed in 10 mm of lead, originally provided to avoid synchrotron-radiation background in the PEP-II application. The outer shell is a magnetic steel cylinder to provide some shielding against stray magnetic fields. In UA9 the detectors are run at 800 to 900V on the PMT and into a discriminator set to 15 mV. The dark rate is a few counts/min under these conditions. Three detectors of this type were installed along the beam line, a pair of them in the proximity of a SPS collimator (not used during 2010 test) and another close to the tungsten absorber region to monitor the losses downstream the RP1 and the LHC collimator.

3.3 GEM chambers

A triple GEM detector is a micro-pattern gas detector which consists of a primary ionization gap and three consecutive GEM foils [18]. A printed circuit board with readout pads detects the current induced by the drifting electron cloud originating from the last GEM stage. Thus the gas amplification and the signal readout are completely separated. The detectors used in SPS layout are built starting from the standard GEM foils produced by CERN with 10×10 cm^2 of active area. The anode PCB 12×12 cm^2 has been designed to house 128 6×12-mm^2 pads inside the active area, while keeping eight connectors for the front end electronics (FEE) in the opposite side placed always in the same position. The three foils are successively glued together forming four gaps (3, 1, 2, 1 mm), following the same structure used for the LHCb chambers [19]. The FEE boards used for this development are based on Carioca-GEM Chip [20] (used for LHCb). The boards, designed and realized at LNF, house 16 ASD channels (2 chips) that produce LVDS time over threshold signals. A mother board finally is plugged just on top of the eight boards for low voltage power supply, threshold distribution, and high voltage filters. The LV supply of 2.5 V and the threshold settings are driven through a NIM module that can be set manually or remotely, through a VME

2011 JINST 6 T10002

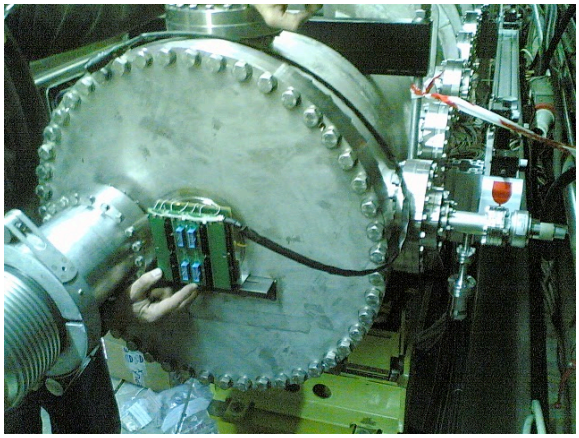

Figure 8. GEM detector during installation on CERN tank (downstream side).

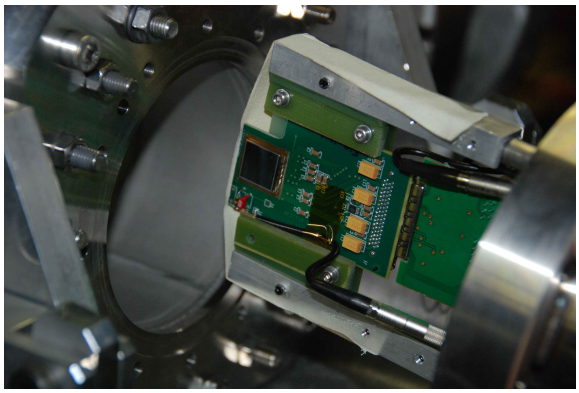

Figure 9. MEDIPIX sensor (black square pad to the left) and readout card to be inserted in RP1. The full assembly, supported by a vacuum flange to the right, is inserted in the Roman pot.

programmable DAC (0÷2 V), while the HV is supplied through a module [21] developed at LNF that starting from a 12 V voltage produces the three GEM voltages (0÷500 V) determining the chamber gain, and the four voltages (0÷1200 V) producing the electric fields for electron cascade drift. The chambers are flushed with a gas mixture $Ar : CO_2 : CF_4$ (45 : 15 : 40).

Two identical triple GEM detectors are installed on the external walls of the CERN tank (figure 8), close to the beam pipe with the anode pads perpendicular to the beam direction. They are therefore sensitive to the secondaries produced in the IHEP tank and in the CERN tank. Those detectors are virtually able to count each single charged particle crossing the sensitive volume. Given the relatively small size of each pad, thresholds can be set at the one mip level. Single pad counting rates in amorphous condition were about 1 KHz. Given the lower threshold the GEM detectors were complementary to the scintillators, being more efficient to count particles with relatively lower rates. Anode current readings proportional to the hit rate are used in online monitoring during data-taking and in offline analysis to compare with rates measured by other BLM.

2011 JINST 6 T10002

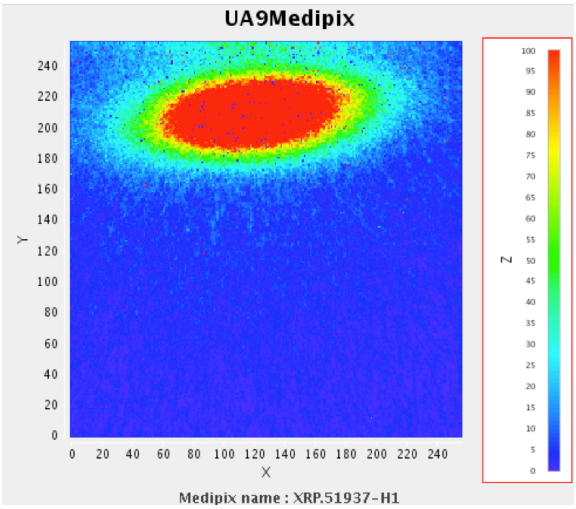

Figure 10. Online Medipix image of the channeled beam. The Y axis corresponds the relative position of the edge of the sensor along the radial direction in the machine horizontal plane. The X axis corresponds to the relative vertical position of the sensor. The axis of the red ellipses are 2.2 and 6.1 mm respectivelly. For each pixel the number of counts Z (proportional to the number of crossing protons) in a gate 1 s long is reported. The full dynamic range for Z is of about 1.1×10^4. In this picture pixels with $Z > 100$ are shown with $Z = 100$.

3.4 Medipix

The Medipix2 MXR ASIC [6] is a high spatial, high contrast resolving CMOS pixel read-out chip working in single photon counting mode. It has originally been designed to be combined with different semiconductor sensors segmented into pixels to detect X-rays and used for X-ray and gamma-ray imaging applications. In UA9 it was used to detect the ionization charge released by the proton crossing the silicon pixels. The preamplified signal from each pixel is discriminated to generate one count. The threshold can be adjusted pixelwise with 4 bits for uniform performance of the whole pixel matrix. Counts are accumulated during a predefined exposure time that can be chosen between few tens μs to several seconds and data are stored in 13-bit counter per pixel. Read-out is performed at the end of the exposure to avoid dead time. In each of the two arms of Roman Pot 1 (RP1) a Medipix detector was installed and used to intercept directly the channeled beam. They have a 1.4×1.4 cm^2 active area segmented in 55×55-μm^2 256×256 pixels. To avoid dead space the board housing the sensor was cut and the edge of the detector put at 1.53 mm from the internal edge of the thin Al window closing the RP1 vacuum vessel (figure 9). Energy calibration of such detectors was done using H8 extracted proton beam and sparse data frames (10-μs long) with crystal in channeling condition. The mean number of counts per hit is about 1.5 with a large uncertainty (20%). In figure 10 a Medipix image with Cr1 in channeling condition for the inner Medipix installed in Roman Pot 1 is shown. The frame exposure time was set at 1 sec. The channeled beam is clearly visible and this guided online data-taking. Offline analysis used these frames to compare with beam lifetime to deduce the extraction efficiency [22]. Besides the two detector in RP1, a third Medipix2 detector has been installed outside the beam pipe in order to monitor beam losses in a region downstream of the crystals.

2011 JINST 6 T10002

3.5 LHC-type BLMs

LHC-type beam loss monitors [23] are ionization chambers with parallel aluminum electrodes separated by 0.5 cm. The detectors are about 50 cm long with a diameter of 9 cm and a sensitive volume of 1.5 liter. The chambers are filled with N_2 at 100 mbar overpressure and operated at 1.5 kV. Their counts are integrated over a 1.2 s period.

Eight LHC BLM were installed in various positions of UA9 experimental region. They were especially useful to detect condition of losses characterized by high rates (100 KHz- 1MHz). When UA9 scintillators tend to saturate, LHC BLM are giving a linear response. On the contrary for relatively low rate (few KHz) they do not provide precise measurements.

3.6 SPS devices

Several SPS devices were available to the UA9 experiment, but they were generally not sensitive to the relatively low current used in the experiment. Some of them were used anyway to measure the beam current and deduce the beam lifetime. Beam Current Transformer (BCT) were pick-up device detecting an induced current due to the passage of the beam particles. The current is integrated over a 10 ms gate and every 16–18 s the information is read out. The SPS current is derived summing the charge information over 1 sec. From time derivative of this measurement the total loss of protons can be derived with some large uncertainty (20–30%). Morevoer, wire scanners were used to measure the emittance of the beam at each fill.

4 Control software and data acquisition

All UA9 devices are controlled via common interface that is able to change positions of the movable devices, to monitor them and to record the rate measurements of the various detectors (figure 11). A powerful middleware is therefore necessary to bring in a single environment data coming from both the machine control system and the UA9 experimental devices, that have conceptually different low level control electronics. The motorization low-level control is based on Labview real-time PXI chassis that talk to the motor drivers or the LVDT transducers through Field Programmable Gate Array (FPGA) cards. All the data from the various devices are in fact coming via different systems and need to be unified and synchronized and then made public over the TCP/IP network (figure 11). A Distributed Information Management (DIM) system used by LHC experiment and capable to connect to different platform is used to collect and send data to various devices through a Front End System Acquisition Architecture (FESA) gateway. The user can connect to the control system via Java application; positions and detector rates are available online through a graphical interface. Every minute the system saves the whole information into text files and guarantees the synchronization.

5 Summary

In this paper we have described the UA9 experimental layout that has been deployed to study the crystal based collimation in the SPS coasting beam at CERN during 2010. Several high precision movable devices were operated in a vacuum environment to orient crystals in the channeling configuration and to check the deflection of the halo protons far from the primary beam. Beam loss

2011 JINST 6 T10002

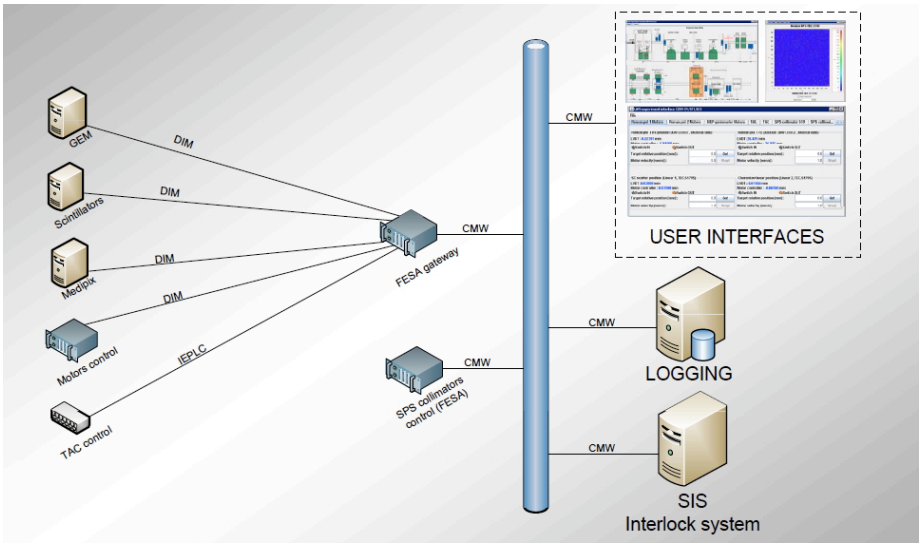

Figure 11. Control and data acquisition scheme.

monitors of various types were used to detect secondary particles produced in inelastic interaction of protons with the accelerator apertures. All this system has been operated in several tests in which the channeling condition was established in a very reproducible way.

Acknowledgments

Work supported by the EuCARD programme GA 227579, within the "Collimators and Materials for high power beams" work package (Colmat-WP8). G. Cavoto and R. Santacesaria acknowledge the support from MIUR (grant FIRB RBFR085M0L 001/I11J10000090001). Some part of this work supported by US DOE under the LARP framework.

References

[1] G. Arduini et al., *Deflection and extraction of Pb ions up to* 33 *TeV/c by a bent silicon crystal.*, *Phys. Rev. Lett.* **79** (1997) 4182;
A.G. Afonin et al., *The schemes of proton extraction from IHEP accelerator using bent crystals*, *Nucl. Instrum. Meth.* **B 234** (2005) 14;
N. Doble, L. Gatignon and P. Grafström, *A novel application of bent crystal channeling to the production of simultaneous particle beams*, *Nucl. Instrum. Meth.* **B 119** (1996) 181.

[2] C.T. Murphy et al., *First results from bent crystal extraction at the Fermilab Tevatron*, *Nucl. Instrum. Meth.* **B 119** (1996) 231;
R.A. Carrigan Jr. et al., *Extraction from TeV-range accelerators using bent crystal channeling*, *Nucl. Instrum. Meth.* **B 90** (1994) 128;
R.A. Carrigan Jr. et al., *Beam extraction studies at* 900 *GeV using a channeling crystal*, *Phys. Rev. ST Accel. Beams* **5** (2002) 043501; *First observation of luminosity-driven extraction using channeling with a bent crystal*, *Phys. Rev. ST Accel. Beams* **1** (1998) 022801;
R.P. Fliller et al., *Results of bent crystal channeling and collimation at the Relativistic Heavy Ion Collider*, *Phys. Rev. ST Accel. Beams* **9** (2006) 013501.

2011 JINST 6 T10002

[3] R.W. Assmann, S. Redaelli and W. Scandale, *Optics study for a possible crystal-based collimation system for the LHC*, in the proceedings of the 10th *biennial European Particle Accelerator Conference (EPAC06)*, June 26–30, Edinburgh, U.K. (2006).

[4] J.B. Jeanneret, *Optics of a two-stage collimation system*, *Phys. Rev. ST Accel. Beams* **1** (1998) 081001.

[5] R.W. Assmann et al., *Designing and building a collimation system for the high-intensity LHC beam*, in the proceedings of the *Particle Accelerator Conference (PAC03)*, May 12–16, Portland, U.S.A. (2003).

[6] M. Campbell, 10 *years of the Medipix2 collaboration*, *Nucl. Instrum. Meth.* **A 633** (2010) S1.

[7] W. Scandale et al., *Probability of inelastic nuclear interactions of high-energy protons in a bent crystal*, *Nucl. Instrum. Meth.* **B 268** (2010) 2655.

[8] A.G. Afonin et al., *High-efficiency beam extraction and collimation using channeling in very short bent crystals*, *Phys. Rev. Lett.* **87** (2001) 094802;
Y.M. Ivanov et al., *Volume reflection of a proton beam in a bent crystal*, *Phys. Rev. Lett.* **97** (2006) 144801.

[9] W. Scandale et al., *Volume reflection dependence of* 400 *GeV/c protons on the bent crystal curvature*, *Phys. Rev. Lett.* **101** (2008) 234801.

[10] S.P. Timoshenko and J.N. Goodier, *Theory of elasticity*, McGraw Hill, U.S.A. (1982).

[11] A.G. Afonin et al., *First results of experiments on high-efficiency single-crystal extraction of protons from the U-*70 *accelerator*, *JETP Lett.* **67** (1998) 781;
S. Baricordi et al., *Low-energy-channeling surface analysis on silicon crystals designed for high-energy-channeling in accelerators*, *Appl. Phys. Lett.* **87** (2005) 094102;
S. Baricordi et al., *Optimal crystal surface for efficient channeling in the new generation of hadron machines*, *Appl. Phys. Lett.* **91** (2007) 061908;
S. Baricordi et al., *Shaping of silicon crystals for channelling experiments through anisotropic chemical etching*, *J. Phys.* **D 41** (2008) 245501.

[12] V. Guidi et al., *Study of anticlastic deformation in a silicon crystal for channeling experiments*, *J. Appl. Phys.* **107** (2010) 113534.

[13] Y.M. Ivanov, A.A. Petrunin and V.V. Skorobogatov, *Observation of the elastic quasi-mosaicity effect in bent silicon single crystals*, *JETP Lett.* **81** (2005) 99.

[14] W. Scandale et al., *Comparative results on collimation of the SPS beam of protons and Pb ions with bent crystals*, *Phys. Lett.* **B 703** (2011) 547.

[15] W. Scandale et al., *High-efficiency deflection of high-energy protons through axial channeling in a bent crystal*, *Phys. Rev. Lett.* **101** (2008) 164801; W. *Observation of nuclear dechanneling for high-energy protons in crystals*, *Phys. Lett.* **B 680** (2009) 129; *Volume reflection dependence of* 400 *GeV/c protons on the bent crystal curvature*, *Phys. Rev. Lett.* **101** (2008) 234801.

[16] E. Bagli et al., *Fabrication of silicon strip crystals for UA*9 *experiment*, in the proceedings of the 1st *international Particle Accelerator Conference (IPAC*10*)*, May 23–28, Kyoto, Japan (2010).

[17] A.S. Fisher, *Instrumentation and diagnostics for PEP-II*, *AIP Conf. Proc.* **451** (1998) 95.

[18] F. Sauli, *GEM: a new concept for electron amplification in gas detectors*, *Nucl. Instrum. Meth.* **A 386** (1997) 531.

2011 JINST 6 T10002

[19] M. Alfonsi et al., *The LHCb triple-GEM detector for the inner region of the first station of the muon system: construction and module-0 performance*, *IEEE Tr. Nucl. Sci.* **53** (2006) 322.

[20] W. Bonivento et al., *Development of the CARIOCA front-end chip for the LHCb muon detector*, *Nucl. Instrum. Meth.* **A 491** (2002) 233.

[21] A. Corradi, F. Murtas and D. Tagnani, *A novel high-voltage system for a triple GEM detector*, *Nucl. Instrum. Meth.* **A 572** (2007) 96.

[22] E. Laface, L. Tlustos and V. Ippolito, *Crystal collimation efficiency measured with the medipix detector in SPS UA9 experiment*, in the proceedings of the 1st *international Particle Accelerator Conference (IPAC10)*, May 23–28, Kyoto, Japan (2010).

[23] M. Stockner et al., , in the proceedings of the 8th *European Workshop on Beam Diagnostics and Instrumentation for Particle Accelerators (DIPAC2007)*, May 20–23, Venice, Italy (2007).

2011 JINST 6 T10002